Journal of Computational Physics 475 (2023) 111839

Contents lists available at ScienceDirect

Journal of Computational Physics

journal homepage: www.elsevier.com/locate/jcp

A hybrid pressure approximation in the control volume finite element method for multiphase flow and transport in heterogeneous porous media

Jumanah Al Kubaisy [a,*], Pablo Salinas [b], Matthew D. Jackson [a]

[a] Novel Reservoir Modelling and Simulation Group, Department of Earth Science and Engineering, Imperial College London, Exhibition Road, London, SW7 2AZ, UK
[b] OpenGoSim, 30 Nelson Street, Leicester, LE1 7BA, UK

ARTICLE INFO

Article history:
Received 25 June 2022
Received in revised form 2 December 2022
Accepted 3 December 2022
Available online 9 December 2022

Keywords:
Hybrid pressure formulation
CVFE methods
Discontinuous permeability
Multiphase flow

ABSTRACT

We present a new hybrid pressure formulation applied to the control volume finite element (CVFE) method to model multiphase flow and transport in highly heterogeneous porous media. The formulation effectively captures sharp saturation changes in the presence of discontinuous material properties by employing a discontinuous pressure approximation at material interfaces. The heterogeneous porous medium is divided into sub-domains within which material properties are uniform or smoothly varying. By construction, the resultant control volume dual mesh is restricted within a sub-domain. The artificial mass leakage across material property boundaries observed in classical CVFE methods is therefore circumvented. The approach applies the robust continuous pressure approximation in the rest of the computational domain; the discontinuous approximation is applied only at the sub-domain boundaries. The discontinuous parameters necessary to achieve mass conservative solutions, locally and globally, are described. We demonstrate the accuracy and efficiency of the new approach by comparison with the classical continuous CVFE method on various examples of heterogeneous domains as well as establishing the convergence of the numerical method. The proposed hybrid formulation significantly outperforms the accuracy and efficiency of classical CVFE methods that use the same order of approximation for modeling multiphase flow in heterogeneous porous media.

1. Introduction

Numerical simulation of multi-phase fluid flow through porous media in the presence of material heterogeneity featuring geometrically complex domains is challenging. Material properties, particularly permeability, can vary by orders of magnitude over very short lengthscales and the boundaries between domains with contrasting properties have complex geometries (e.g. [22,14,24]). The control volume finite element (CVFE) method is inherently flexible for modeling multiphase flow and transport in such complex porous media, and is well documented in the literature [20,21,16,17,25,8,18,22,28,36,26,23,35,38]. The approach combines the finite element method that resolves flow for elliptic or parabolic problems on geometrically complex, unstructured meshes with the stable and mass conservative finite volume method for resolving the

* Corresponding author.
E-mail address: j.al-kubaisy19@imperial.ac.uk (J. Al Kubaisy).

https://doi.org/10.1016/j.jcp.2022.111839

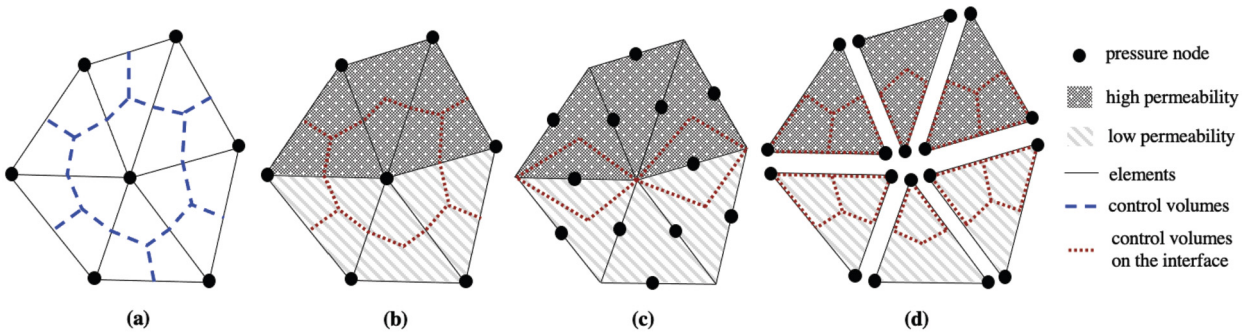

Fig. 1. **(a)** Node centered control volume dual mesh construction. **(b-d)** Comparison of control volume discretizations along a discontinuous material interface: **(b)** Classical control volume finite element method. **(c)** Interface control volume finite element method [4]. **(d)** $P_{2(DG)} - P_{1(DG)}$ element-pair of [35].

hyperbolic transport problem [16,22]. Alternatively, the finite volume (FV) method is used to model flow in porous media, discretized using *k*-orthogonal grids and applying the two point flux approximation [34,7,15]. This approach is fast and robust but suffers from grid orientation errors and requires very high grid resolution when used to simulate multiphase flow through geometrically complex geological features [26]. Extension of the FV method to unstructured meshes can be achieved using the multi-point flux approximation (MPFA) [2,3,6]. The MPFA provides a general discretization framework for modeling flow on non-*k*-orthogonal grids by introducing additional points in the cell stencil. The approach has limitations due to the added computational cost of a large stencil and the potential for instabilities to develop when modeling multiphase flow through heterogeneous and anisotropic porous media [1].

The family of mixed finite element (MFE) methods offers a flexible approach to simulate flow in heterogeneous subsurface domains [11–13,17,25]. In the MFE method, the flow variables are estimated using an element-wise constant approximation for pressure and the lowest order Raviart-Thomas (RT) approximation for velocity. Since the fluxes are continuous between elements, the transport is resolved on the same element mesh, ensuring a mass conservative solution [17]. The main drawbacks of the approximation are (i) the increased computational cost: it requires between 1.5 to 4 times the degrees of freedom (DoF) used by the CVFE method [17,22] and (ii) the indefinite matrices assembled by the set of equations [17]. The mixed-hybrid finite element (MHFE) method addresses the latter issue by the introduction of additional trace variables [29,13]. More recently, the mimetic finite difference (MFD) method extended the MHFE approach to discretize any polygonal shape by the numerical evaluation of the shape function [5]. The development of the MFD method for flow in porous media applications is described by several authors (e.g. [32,40,41,5,30]).

In the CVFE approach, the discretization of primary flow and transport variables is based on two meshes, the element (primary) mesh and the control volume (dual) mesh. The element mesh describes the material properties that can vary element-wise (i.e. permeability) while the control volumes are centered on the vertices of the elements [21,22,26]. Fig. 1a highlights the construction of the control volume mesh. When neighbouring elements contain contrasting material properties (i.e. they lie on either side of a sharp boundary such as a fracture wall; Fig. 1b), the shared control volumes that span these elements allow mass to 'leak' across the boundary, contaminating the multiphase transport solution [19,35]. Consequently, the heterogeneous model is not honored.

Several methods have been developed to reduce or eliminate this numerical mass leakage. Abushaikha et al. [4] proposed the interface control volume finite element (ICVFE) method by globally applying the pressure discretization on the element edges rather than the element vertices in order to reduce the size of the overlap across elements. The control volumes constructed by this approach span at most two adjacent elements (Fig. 1c). The method is effective in reducing numerical leakage; however, it does not eliminate the issue entirely and is numerically expensive. Salinas et al. [35] employed a global discontinuous Galerkin discretization for pressure. In the Salinas et al. [35] method, the element pair $P_{2,DG} - P_{1,DG}$ was used: velocity and pressure are approximated using discontinuous Galerkin of second order and first order, respectively. The control volumes in this discretization are discontinuous across all element edges (Fig. 1d). The technique is highly effective in preventing numerical leakage without mesh refinement at discontinuities. The drawback of this approach is that it is numerically expensive as a result of the global duplication of pressure and velocity nodes and the higher order velocity approximation required to ensure stability. Thus, the method requires solution of a large system of equations.

Nick and Matthäi [31] presented a discontinuity finite element finite volume method (DFEFVM) that was initially developed for single phase flow and passive solute transport. The approach prevents control volume overlap across discontinuous interfaces by incorporating additional pressure nodes while using the continuous approach elsewhere. The method was later extended by Tran et al. [38] to capture capillary barriers in two phase flow problems. Strong coupling of pressure nodes across capillary discontinuities is carried out as a pre-processing step by modifying the system of equations based on the likelihood of fluid movement across the interface. Furthermore, they employed an interface condition, described by van Duijn and de Neef [39], to determine the saturation along the capillary barrier. The approach targeted capillary interface coupling at discontinuities and has not been generalized further.

The aim of this work is to develop a hybrid control volume finite element (HyCVFE) method that selectively applies a discontinuous pressure approximation along the boundaries of contrasting material sub-domains while the continuous approximation is exploited in the rest of the domain where material properties are constant or smoothly varying. The method is designed to effectively and accurately capture multiphase fluid flow within and between highly heterogeneous sub-domains with contrasting material properties without compromising the robustness of the numerical approximation or significantly increasing computational cost compared to the classical CVFE method. The paper is organized as follows. In Section 2 the governing equations of the multiphase model are described. Section 3 details the mathematical derivation of the hybrid approach for the coupled multiphase flow and transport equations and then describes the solution method and other approximations employed in the implementation of the HyCVFE method. We validate the method and demonstrate its effectiveness with numerical experiments in Section 4. Finally, conclusions are drawn in Section 5.

2. Governing equations

Consider Darcy's law that describes fluid flow through porous media. The total fluid Darcy velocity ($\mathbf{v_t}$) is given by

$$\mathbf{v_t} = -\lambda_t \mathbf{K} \cdot \nabla p + \mathbf{f}, \tag{1}$$

where $\mathbf{K}$, ∇p, and $\mathbf{f}$ are the permeability tensor, the pressure gradient, and a term accounting for capillary and gravity forces, respectively. For a two phase system, the total mobility (λ_t) is the summation of the wetting phase mobility (λ_w) and the non-wetting phase mobility (λ_{nw}) as

$$\lambda_t = \frac{k_{r,w}(S_w)}{\mu_w} + \frac{k_{r,nw}(S_w)}{\mu_{nw}}. \tag{2}$$

Here k_r is the relative permeability, that is a function of the saturation S_w, and μ is the fluid viscosity. The subscripts w and nw denote the wetting and non-wetting phases, respectively. The continuity equation of the incompressible system is given by

$$\nabla \cdot \mathbf{v_t} = q_t, \tag{3}$$

where q_t denotes a source term. Now consider the fractional flow form of the mass balance equation for the wetting phase

$$\phi \frac{\partial S_w}{\partial t} + \nabla \cdot (f_w \mathbf{v_t}) = q_w, \tag{4}$$

where ϕ is the porosity of the medium, S_w is the wetting phase saturation, t is time and q_w is a source term for the wetting phase. The fractional flow of phase α (f_α) is given by

$$f_\alpha = \frac{\lambda_\alpha}{\lambda_t}. \tag{5}$$

We solve the mass balance equation for the unknown saturation subject to

$$S_w + S_{nw} = 1, \tag{6}$$

in order to constrain the total volume fraction.

3. Method

3.1. Formulation of the flow equations

3.1.1. Finite element method

The finite element method is used to solve the flow problem. First, the computational domain Ω is partitioned into a set of n_d sub-domains, $\{\Omega_d\}_{d\in[1,n_d]}$ (Fig. 2). Each sub-domain (Ω_d) defined by its homogeneous or smoothly varying material properties, following the approach of Jacquemyn et al. [27] and Osman et al. [33], and triangulated into $n_{d,e}$ elements such that ($\mathcal{T}_d = \cup_{e=1}^{n_{d,e}} \Omega_e$) using a constrained conforming Delaunay triangulation [37]. We use the element pair $P_{0,DG} - P_{1,H}$ to discretize velocity and pressure. The velocity vector is approximated using a discontinuous element-wise representation. The pressure approximation is hybrid by having a continuous, first order polynomial representation within each sub-domain (Ω_d), but a discontinuous representation along the boundaries of the sub-domain (Γ_d) (Fig. 2). Let

$$\mathbf{v_t}(\mathbf{x}) = \sum_{j\in\Omega} \mathbf{\Phi}_j(\mathbf{x}) v_{t,j}, \tag{7}$$

and

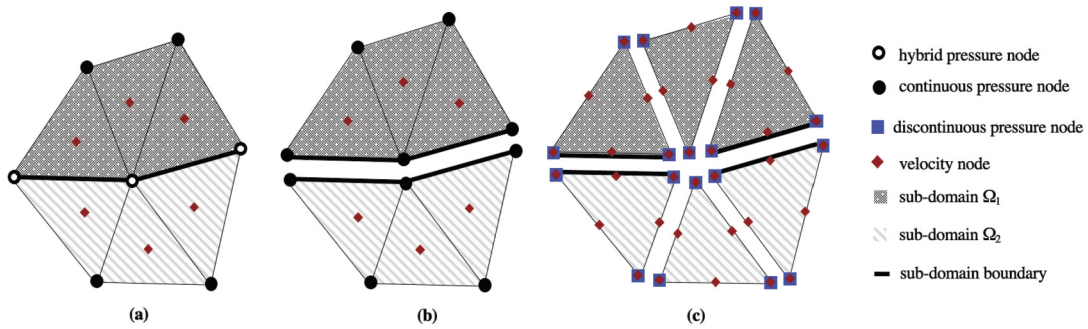

Fig. 2. (**a**) Discretization of pressure and velocity on a mesh using the HyCVFE method with two sub-domains Ω_1 and Ω_2. Emphasis is placed on the hybrid pressure nodes lying on the sub-domain boundary. (**b**) Internal splitting of the hybrid pressure nodes along the sub-domain boundary. A continuous pressure approximation is applied within each sub-domain while the necessary discontinuous approximations are used to establish the connections between sub-domains. (**c**) Discretization of the pressure and velocity using the high order discontinuous method of Salinas et al. [35].

$$p_d(\mathbf{x}) = \sum_{j \in \Omega_d} \Psi_j(\mathbf{x}) p_j, \qquad \forall d \in [1, n_d] \tag{8}$$

be the approximations of the total velocity and pressure fields. $\mathbf{\Phi}(\mathbf{x})$ and $\Psi(\mathbf{x})$ are the basis functions of velocity and pressure, respectively, while v_t and p are the unknown coefficients. The hybrid approach is applied on the sub-domain boundaries by incorporating additional pressure nodes that separate the sub-domains (Fig. 2 (a-b)). Consequently, the nodes are continuous within each sub-domain and the discontinuous pressure approximation is applied only between the sub-domains to establish the global flow model. Fig. 2 (b-c) emphasizes the differences between the discretization employed here in the proposed HyCVFE method and the discontinuous method of Salinas et al. [35]. In the latter approach, the velocity and pressure degrees of freedom placed on the element boundaries are duplicated for neighbouring elements (Fig. 2c). Moreover, the approach of Salinas et al. [35] employed a second order discontinuous velocity approximation that was necessary to ensure stable solutions.

3.1.2. Discretization of Darcy's equation

The weak form of Eqn. (1) is obtained by weighting with the test function $\mathbf{\Phi_i}$, derived from the same space as the velocity basis functions, and integrating over the domain

$$\int_{\Omega} \mathbf{\Phi_i} \cdot \mathbf{v}_t \, d\Omega + \int_{\Omega} \mathbf{\Phi_i} \cdot \left(\lambda_t \mathbf{K} \cdot \nabla p\right) d\Omega = 0. \tag{9}$$

Equivalently, the domain (Ω) is decomposed of n_d sub-domains, given by

$$\sum_{\Omega_d \in \Omega} \left[\int_{\Omega_d} \mathbf{\Phi_i} \cdot \mathbf{v}_t \, d\Omega_d + \int_{\Omega_d} \mathbf{\Phi_i} \cdot \left(\lambda_t \mathbf{K} \cdot \nabla p\right) d\Omega_d \right] = 0, \tag{10}$$

where the term accounting for capillarity and gravitational forces is neglected. Applying integration by parts on the second term, yields

$$\sum_{\Omega_d \in \Omega} \left[\int_{\Omega_d} \mathbf{\Phi_i} \cdot \mathbf{v}_t \, d\Omega_d - \int_{\Omega_d} \nabla \left(\mathbf{\Phi_i} \cdot \lambda_t \mathbf{K}\right) p \, d\Omega_d + \int_{\Gamma_d} \left(\mathbf{\Phi_i} \cdot \lambda_t \mathbf{K} p\right) \cdot \mathbf{n} \, d\Gamma_d \right] = 0. \tag{11}$$

In order to accommodate the pressure discontinuity between sub-domains in the approximation, we apply integration by parts one more time on the second term. This approach is adapted from Salinas et al. [35] and applied exclusively on Γ_d

$$\sum_{\Omega_d \in \Omega} \left[\int_{\Omega_d} \mathbf{\Phi_i} \cdot \mathbf{v}_t \, d\Omega_d + \int_{\Omega_d} \left(\mathbf{\Phi_i} \cdot \lambda_t \mathbf{K}\right) \cdot \nabla p \, d\Omega_d - \int_{\Gamma_d} \left(\mathbf{\Phi_i} \cdot \lambda_t \mathbf{K} \tilde{p}\right) \cdot \mathbf{n} \, d\Gamma_d + \int_{\Gamma_d} \left(\mathbf{\Phi_i} \cdot \lambda_t \mathbf{K} p\right) \cdot \mathbf{n} \, d\Gamma_d \right] = 0, \tag{12}$$

where p and $\tilde{p}$ in the last two terms on the left hand side correspond to the pressure nodes that share the same coordinates on the discontinuous interface (Γ_d). We substitute the finite element approximations for the velocity and pressure, Eqns. (7) and (8), and apply the finite element triangulation ($\mathcal{T}_d$) over each sub-domain

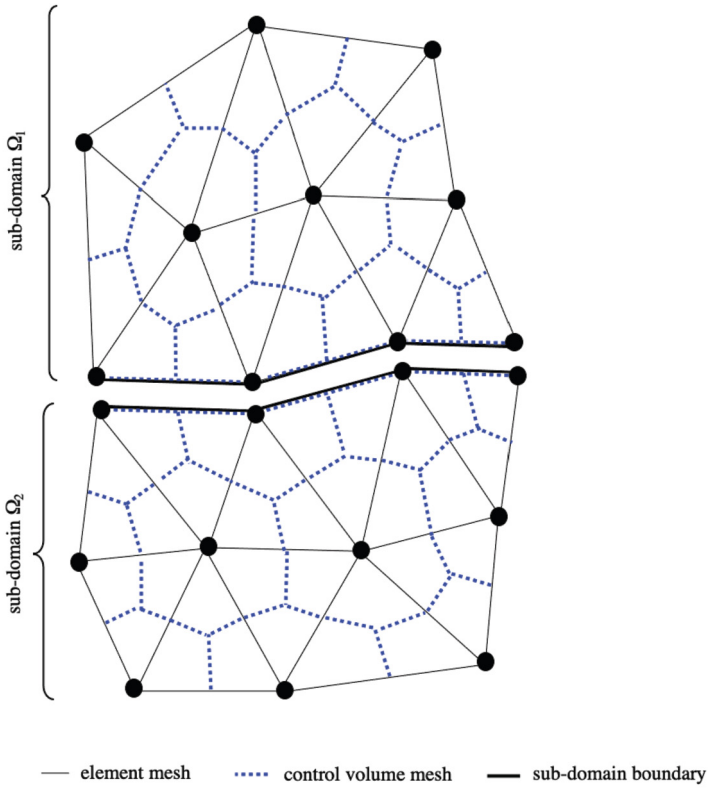

Fig. 3. The dual mesh construction in the presence of hybrid pressure nodes. The control volumes are separated along the discontinuous interface.

$$\sum_{\Omega_d\in\Omega}\Bigg[\sum_{\Omega_e\in\Omega_d}\sum_{j=1}^{n_{d,v}}\int_{\Omega_e}\boldsymbol{\Phi}_{\mathbf{i}}\cdot\boldsymbol{\Phi}_{\mathbf{j}}v_{t,j}\,d\Omega_e+\sum_{\Omega_e\in\Omega_d}\sum_{k=1}^{n_{d,p}}\int_{\Omega_e}\left(\boldsymbol{\Phi}_{\mathbf{i}}\cdot\lambda_t\mathbf{K}\right)\cdot\nabla\Psi_k p_k\,d\Omega_e + \sum_{\Gamma_e\in\Gamma_d}\sum_{k=1}^{n_{e,p}}\oint_{\Gamma_e}\left(\boldsymbol{\Phi}_{\mathbf{i}}\cdot\lambda_t\mathbf{K}_h\Psi_k\left(p_k-\tilde{p}_k\right)\right)\cdot\mathbf{n}\,d\Gamma_e\Bigg]=0, \tag{13}$$

where $n_{d,v}$, $n_{d,p}$, and $n_{e,p}$ are the number of velocity nodes in sub-domain Ω_d, the number of pressure nodes in sub-domain Ω_d, and the number of hybrid pressure nodes on the discontinuous interface (Γ_d), respectively. $\mathbf{K}_h$ denotes the harmonic average of the permeability on the discontinuous interface (Γ_d), Ω_e is the element, and Γ_e is the element boundary. Eqn. (13) describes the system of equations of all the sub-domains that are coupled by hybrid pressure nodes across their shared interfaces (Γ_d). The last term on the left-hand side in Eqn. (13) is nonzero for the hybrid nodes such that $\tilde{p}$ is the hybrid pressure node of p that lies on the sub-domain boundary.

3.1.3. Discretization of the continuity equation

Our approach to discretize the continuity equation on the control volume dual mesh follows [26,23]. Fig. 3 highlights the construction of control volumes along the sub-domain boundaries (Γ_d). The hybrid pressure nodes provide restricted control volumes, with limited support, to their respective sub-domains. Consequently, no two adjacent sub-domains share a control volume. We derive the weak form of Eqn. (3) by weighting with the test function Ψ_i, from the space of the pressure basis functions, and integrating over the domain (Ω)

$$\sum_{\Omega_d\in\Omega}\left[\int_{\Omega_d}\Psi_i\nabla\cdot\mathbf{v}_t\,d\Omega_d-\int_{\Omega_d}\Psi_i q_t\,d\Omega_d\right]=0. \tag{14}$$

Substituting the finite element approximation to the weak form gives

$$\sum_{\Omega_d\in\Omega}\left[\sum_{\Omega_{cv}\in\Omega_d}\sum_{j=1}^{n_{d,v}}\int_{\Omega_{cv}}\Psi_i\nabla\cdot\boldsymbol{\Phi}_{\mathbf{j}}v_{t,j}\,d\Omega_{cv}-\sum_{\Omega_{cv}\in\Omega_d}\int_{\Omega_{cv}}\Psi_i q_t\,d\Omega_{cv}\right]=0, \tag{15}$$

with Ω_{cv} representing the control volume. Applying the divergence theorem on the first term yields

$$\sum_{\Omega_d \in \Omega} \Bigg[\sum_{\Gamma_{cv} \in \Omega_d \setminus \Gamma_d} \sum_{j=1}^{n_{d,v}} \int_{\Gamma_{cv}} \Psi_i \left(\mathbf{\Phi_j} v_{t,j} \right) \cdot \mathbf{n} \, d\Gamma_{cv} + \sum_{\Gamma_{cv} \in \Gamma_d} \sum_{j=1}^{n_{d,v}} \int_{\Gamma_{cv}} \Psi_i \left(\mathbf{\Phi_j} \tilde{v}_{t,j} \right) \cdot \mathbf{n} \, d\Gamma_{cv} - \sum_{\Omega_{cv} \in \Omega_d} \int_{\Omega_{cv}} \Psi_i q_t \, d\Omega_{cv} \Bigg] = 0, \tag{16}$$

where $\tilde{v}_{t,j}$ and Γ_{cv} denote the harmonic permeability-weighted velocity on the discontinuous interface (Γ_d), and the control volume boundary. Here, we separated the internal fluxes of the sub-domain from the external fluxes (Fig. 4). The second term in Eqn. (16) is non-zero for control volumes that lie on the sub-domain boundaries, contributing to external fluxes. The term ensures continuity of the fluxes across the global domain.

3.2. Formulation of the transport equation

Finite-volume discretization

We discretize the mass balance equation in space over each control volume and in time using forward Euler, then apply the divergence theorem to obtain the surface integral of the velocity term in Eqn. (4). The linearized integral-form of the transport equation for the wetting phase is given by

$$\int_{\Omega_{cv}} \frac{\phi (S^{n+1}_{w,cv} - S^{n}_{w,cv})}{\Delta t} \, d\Omega_{cv} = - \oint_{\Gamma_{cv}} \left(f^{n}_{w,cv} \mathbf{v}^{n+1}_{t} + \frac{\partial f_{w,cv}}{\partial S_{w,cv}} \Bigg|^{n} (S^{n+1}_{w,cv} - S^{n}_{w,cv}) \mathbf{v}^{n+1}_{t} \right) \cdot \mathbf{n} \, d\Gamma_{cv} + \int_{\Omega_{cv}} q_w \, d\Omega_{cv}, \tag{17}$$

where Δt is the time step size and the superscripts n and $n+1$ denote the current and next time steps, respectively. Eqn. (17) describes the mass balance equation of the wetting phase applied to any control volume in the domain to approximate the saturation (S_w).

3.3. Solution method

We couple the flow and transport equations using an Implicit Pressure Explicit Saturation (IMPES) scheme. This approach is appropriate in the context of CVFE methods due to the sequential nature of the formulation combined with the ease of implementation for testing and validation. In our implementation, the pressure and velocity are obtained implicitly by solving the finite element flow problem while keeping the saturation field unchanged. Then the saturation is updated explicitly on the control volume mesh [16,22]. The explicit time stepping only guarantees stability for sufficiently small time steps, when the Courant–Friedrichs–Lewy (CFL) number does not exceed unity [7]. The numerical method is implemented in a proof of concept code for two-dimensional models using Python with the finite element mesh generated using CoreForm's Cubit software.

3.3.1. Implicit pressure solution

Consider the global system of equations assembled from the force-balance given by Darcy's law and the continuity equation, Eqn. (13) and (16), respectively. The algebraic system can be written as

$$\begin{bmatrix} \mathbf{A} & \mathbf{B} \\ \mathbf{C} & \mathbf{0} \end{bmatrix} \cdot \begin{bmatrix} \mathbf{v}^{n+1}_{t} \\ p^{n+1} \end{bmatrix} = \begin{bmatrix} b_1 \\ b_2 \end{bmatrix} \tag{18}$$

A is the mass matrix and in this specific formulation is a diagonal matrix. **B** and **C** are the stiffness matrix and the divergence-free velocity operator, respectively. Both of these are composed of two terms. The stiffness matrix (**B**) is composed of the last two terms on the LHS of Eqn. (13). The second term has a block diagonal structure for each sub-domain, while the third is the jump-term attributing to fill-ins in the off block-diagonal structure. Similarly, **C** is composed of the first two terms on the LHS of Eqn. (16). The first term accounts for internal fluxes within each sub-domain, while the second term accounts for external fluxes between sub-domains ensuring continuity of the model.

The coupling term in the flow equation is the total mobility (λ_t), described in Eqn. (2), that must be updated in the stiffness matrix (**B**) prior to solving the flow unknowns for each time step. The saturation-dependence of the relative permeability introduces strong non-linearities in the formulation [7]. In the proposed method, we approximate it using upstream weighted values to maintain stable and physical solutions. The velocity and pressure can be solved simultaneously using this formulation. We use a projection-based method to eliminate the velocity unknown and solve first for the pressure, similar to the approach used in Jackson et al. [26] and Salinas et al. [35]. The velocity is then determined from the first row in Eqn. (18) by substituting the pressure solution.

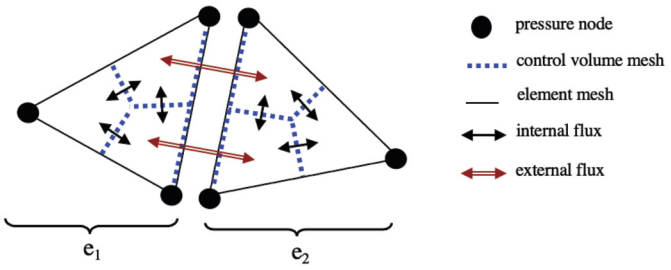

Fig. 4. Types of fluxes in the hybrid model. The single and double arrows highlight internal fluxes within an element and external fluxes through discontinuous interface connecting e_1 with e_2, respectively.

3.3.2. Interface approximations

When updating the saturation using Eqn. (17), we consider two fluxes (Fig. 4): the internal flux between control volumes within the same sub-domain, and the external flux between control volumes in different elements in neighbouring sub-domains (Fig. 4). Internal fluxes are straightforward to compute since the control volume interface is internal to the element and the flux is constructed to be continuous within each element. To establish consistent external flux approximations, we refer to the discretization of the continuity equation, Eqn. (16), which computes the harmonic permeability-weighted velocity at sub-domain boundaries ($\tilde{\mathbf{v}}_t$) given by

$$\tilde{\mathbf{v}}_t = \frac{1}{2}\left(\mathbf{K}_h\mathbf{K}_{e_1}^{-1}\mathbf{v}_{t,e_1} + \mathbf{K}_h\mathbf{K}_{e_2}^{-1}\mathbf{v}_{t,e_2}\right), \tag{19}$$

where $\mathbf{K}_h$, $\mathbf{K}^{-1}$, and $\mathbf{v}_t$ are the harmonic weighted permeability, the inverse of the element's permeability, and the element's velocity, respectively. The approximation described here is similar but not identical to the one used by Gomes et al. [23] and Salinas et al. [35]. We differ by not incorporating the weighted volumes in the flux approximation. Our numerical experiments show that this approximation provides locally mass conservative scheme. The fractional flow term (f_w) and its partial derivative with respect to saturation $\left(\frac{\partial f_w}{\partial S_w}\right)$ are approximated, similar to the total mobility term described earlier, by using upstream weighted values.

4. Numerical experiments

We first verify the steady state pressure solution for single phase flow in test Case 4.1. We next validate and establish the convergence of the HyCVFE formulation for two phase flow using the Buckley-Leverett problem in test Case 4.2. We then demonstrate the advantages of the proposed method compared to the classical CVFE method and the discontinuous method of Salinas et al. [35] using three heterogeneous test cases. Test Cases 4.3 and 4.4 consider two phase flow in a single fracture model, and an embedded box model, that were used previously [4,35]. The final test case, 4.5, represents a highly challenging example in which two phase flow is focused into a fracture tip embedded in a low permeability domain.

We report the degrees of freedom in the numerical examples using

$$N_{CVFE} = N_p + N_v + N_s, \tag{20}$$

for the continuous method where N_p, N_v, N_s are the pressure, velocity, and saturation degrees of freedom. For the hybrid method we use

$$N_{HyCVFE} = \sum_{\Omega_d \in \Omega} \left(n_{d,p} + n_{d,v} + n_{d,s}\right), \tag{21}$$

where $n_{d,p}$, $n_{d,v}$, and $n_{d,s}$ are the pressure, velocity, and saturation degrees of freedom in sub-domain Ω_d. In single phase flow problems, the saturation degrees of freedom in Eqn. (20) and Eqn. (21) are neglected. In multiphase numerical experiments, we use the Brooks-Corey model [9] that describes the relative permeability curves by

$$k_{rw}(S_w) = \left(\frac{S_w - S_{w,r}}{1 - S_{w,r} - S_{nw,r}}\right)^{n_w}, \tag{22}$$

and

$$k_{rnw}(S_w) = \left(\frac{1 - S_w - S_{nw,r}}{1 - S_{w,r} - S_{nw,r}}\right)^{n_{nw}}, \tag{23}$$

where the superscript n is the Corey exponent, and $S_{\alpha,r}$ is the residual saturation of phase α. The parameters for each model are provided in Table 1.

Table 1
Summary of model setup.

	4.1	4.2	4.3	4.4	4.5
L_x	1.	1.	1.	1.	1.
L_y	0.05	0.05	0.25	1.	0.5
ϕ	0.1	0.1	0.1	0.1	0.1
n_w	N/A	2.	2.	2.	2.
n_{nw}	N/A	2.	2.	2.	2.
$S_{w,r}$	N/A	2.	2.	2.	2.
$S_{nw,r}$	N/A	0.3	0.3	0.3	0.3
$\mathbf{K}_{high}/\mathbf{K}_{low}$	2.	N/A	10^4	10^4	10^6
μ_{nw}/μ_n	N/A	2.	2.	2.	2.

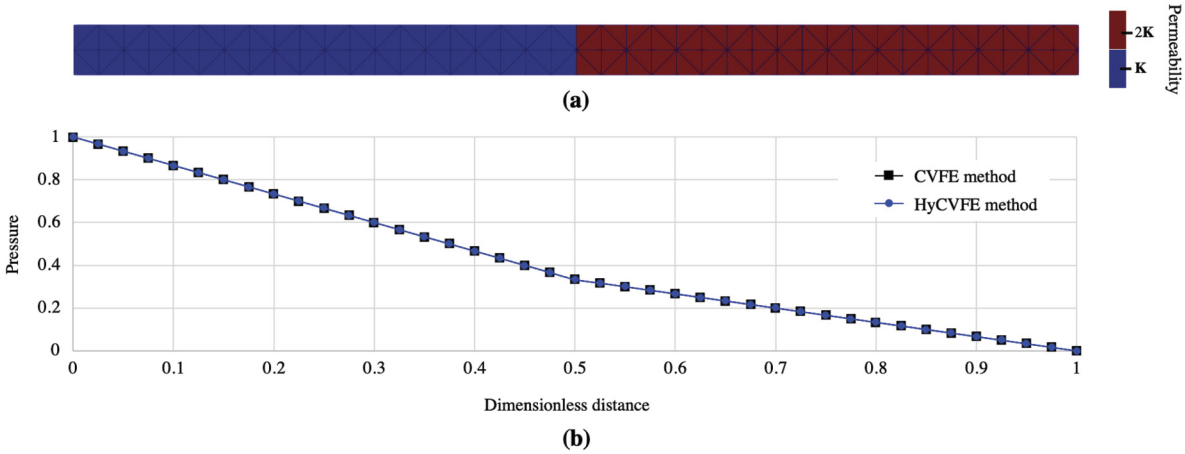

Fig. 5. Steady-state pressure test case (4.1): (**a**) The heterogeneous permeability field on the finite element mesh. (**b**) Comparison of the pressure distribution along the horizontal axis for the CVFE and the HyCVFE methods. Hybrid pressure nodes yield the correct pressure solution at discontinuities.

We adapt the approach used by Salinas et al. [35] to compare the fraction of mass leakage (ϵ_{max}) obtained using different approximations. The normalised mass leakage ϵ_{max} measures the undesired change in wetting phase saturation due to leakage and is defined as

$$\epsilon_{max} = \frac{\sum_{i\in\Omega_{low}} \left(S_{w,i} - S_{w,r,i}\right)\Omega_{cv,i}}{\sum_{i\in\Omega_{low}} \Omega_{cv,i}} \tag{24}$$

where Ω_{low} refers to the low permeability sub-domain into which numerical mass leakage is of concern.

4.1. Steady-state pressure

We validate the pressure solution for single phase flow in a heterogeneous porous medium in the presence of hybrid pressure nodes. The permeability field projected onto the finite element mesh is shown in Fig. 5(a); the high permeability sub-domain to the right has twice the permeability of the low permeability subdomain to the left (Table 1). The HyCVFE method mesh is decomposed into two sub-domains such that hybrid pressure nodes are placed at $x = 0.5$. N_{CVFE} and N_{HyCVFE} required to solve the flow model are 443 and 446, respectively. Fig. 5(b) compares the pressure profile along the horizontal axis for the two methods. The pressure drop in the higher permeability region to the right correctly corresponds to half the slope of the pressure drop exhibited in lower permeability region to the left. Moreover, hybrid pressure nodes yield the correct pressure approximation at the discontinuity, $x = 0.5$. The test case demonstrates that the proposed method provides the correct pressure solution.

4.2. Buckley-Leverett problem

We validate the coupled flow and transport solution of the HyCVFE method against the semi-analytical Buckley-Leverett solution [10]. The model setup is as follows. In the absence of gravity and capillary forces, the homogeneous medium is initially saturated with the non-wetting phase, which is then displaced by the wetting phase. For validation purposes, we introduce multiple discontinuous interfaces in the homogeneous medium to test the hybrid pressure nodes, resulting in 8 sub-domains. Fig. 6a shows the two-dimensional mesh used in this numerical example with 40 elements along the x-axis ($n_x = 40$). The dashed red lines represent discontinuous interfaces at which control volumes do not span element

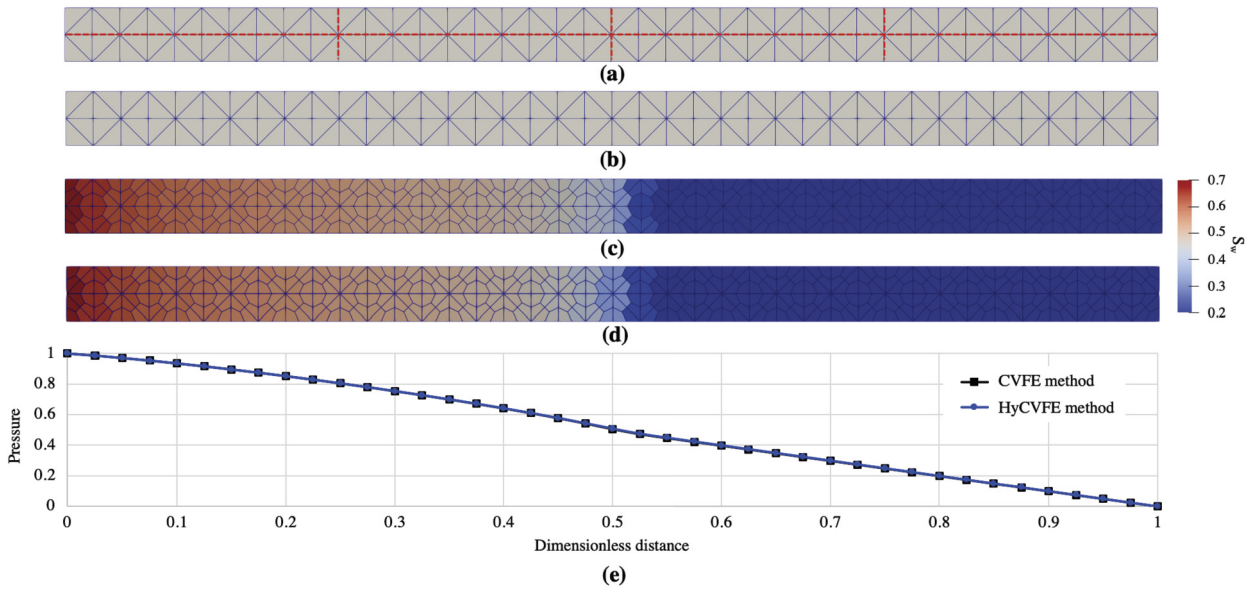

Fig. 6. Pseudo one-dimensional numerical Buckley-Leverett test case (4.2). (**a**) HyCVFE method element mesh with red dashed lines indicating discontinuous interfaces. (**b**) Reference CVFE method element mesh. The saturation solution after 0.2 PVI is displayed CV-wise for (**c**) the HyCVFE method and (**d**) the CVFE approach. (**e**) Comparison of the corresponding pressure solution for CVFE and HyCVFE methods. (For interpretation of the colours in the figure(s), the reader is referred to the web version of this article.)

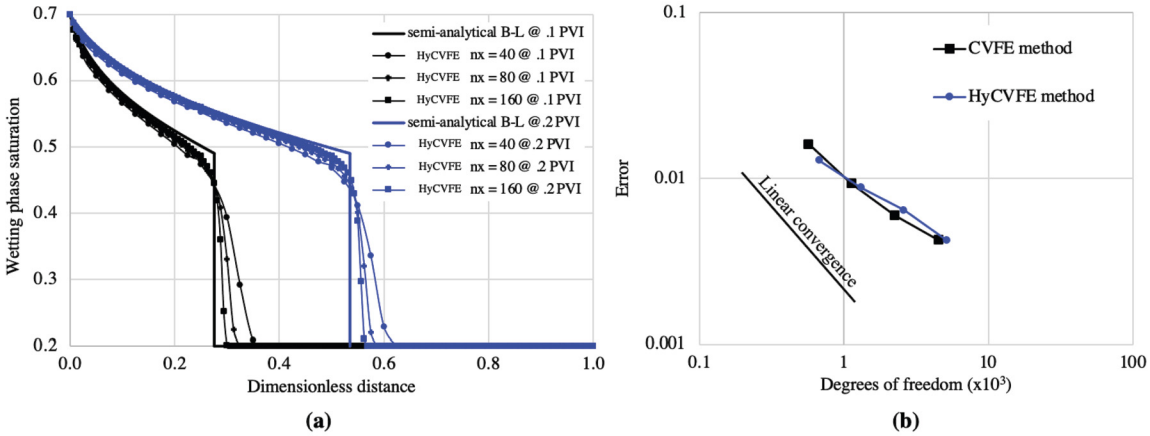

Fig. 7. Convergence of the numerical solution to the semi-analytical Buckley-Leverett (B-L) test case (4.2): (**a**) Comparison of the proposed, hybrid method to the semi-analytical B-L after 0.1 and 0.2 PVI. (**b**) L1-norm of the error for the HyCVFE and classical CVFE approximations.

boundaries. The numerical saturation solution after 0.2 pore volumes injected (PVI), obtained using the classical CVFE and our HyCVFE approach is shown in Fig. 6. The saturation obtained using our HyCVFE method is in good agreement with the classical CVFE. The corresponding pressure distribution deviates from a linear gradient in the interval $x \in [0, 0.5]$ due to the quadratic relative permeability curves. Again, the CVFE and HyCVFE results are in good agreement.

We demonstrate the convergence of the proposed method to the semi-analytical solution of the Buckley-Leverett problem after 0.1 and 0.2 PVI in Fig. 7a. The saturation profile shows several numerical solutions obtained with different mesh resolutions ($nx = 40, 80, 160$) compared with the semi-analytical solution. We observe that refinement of the mesh results in a better agreement with the semi-analytical solution. In all cases, the area under the semi-analytical and numerical curves represents the same mass of wetting phase injected into the model. The flux continuity approach employed in the HyCVFE method guarantees local and global mass conservation. The L1-norm of the error shows the rate of convergence of the numerical methods, which is close to linear (Fig. 7b). The additional nodes introduced at discontinuous interfaces in the HyCVFE approach introduce additional degrees of freedom that result in a slight shift of the curve for the HyCVFE method to the right when compared to the reference CVFE method.

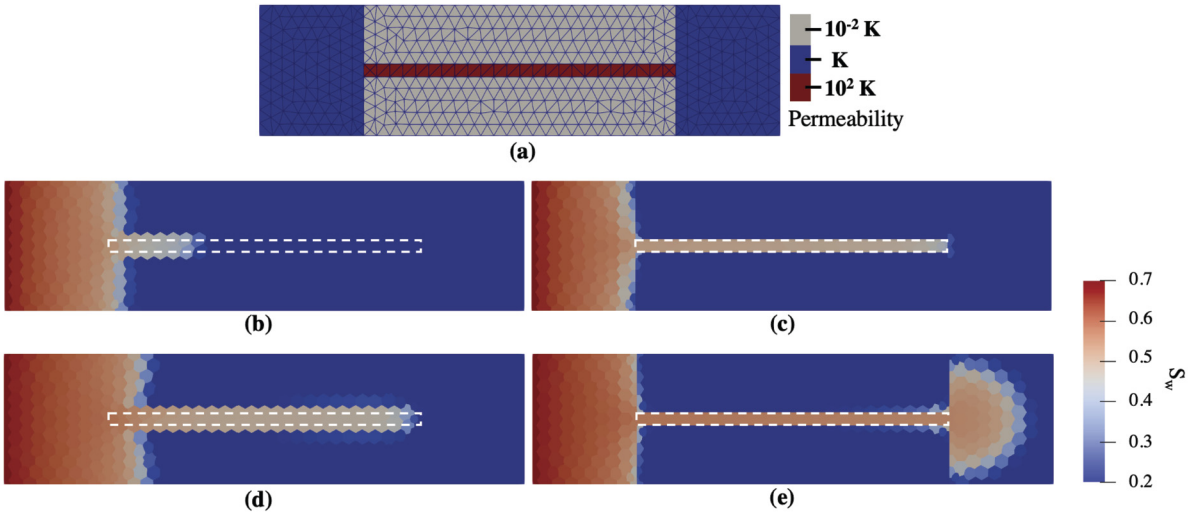

Fig. 8. (**a**) The permeability field of the single fracture test case (4.3). The fracture is enclosed in a low permeability zone above and below while the left and right boundaries include intermediate permeability zones. (**b** – **e**) Comparison of the saturation solution displayed using the control volume representation. The left column shows the CVFE method while the right column shows the HyCVFE method. (**b**) and (**c**), (**d**) and (**e**) display the solution after 0.1 and 0.14 PVI, respectively. The dashed box in the plots outlines the fracture zone.

4.3. Single fracture problem

We demonstrate the potential of the method to reduce numerical mass leakage with a two-dimensional example from Abushaikha et al. [4] and Salinas et al. [35]. A narrow conductive zone, representing a fracture, is enclosed in low permeability zones (Table 1). This case shows the performance of the HyCVFE method with multiple sub-domain interfaces with different material property contrasts and interface orientations with respect to the flow. The permeability field is shown in Fig. 8a. The fracture sub-domain consists of a thin layer of elements. The model features intermediate permeability zones to the right and left of the fracture sub-domain where pressure boundary conditions are applied. The model is initially saturated with the non-wetting phase, and the wetting phase is injected from the left boundary to displace the non-wetting phase through the right boundary. We compare the accuracy of the saturation solution at several timesteps in Fig. 8(b-e) for the HyCVFE approach and the reference CVFE method. The saturation profiles differ between the two methods because the CVFE approach suffers from numerical leakage from the fracture into the surrounding low permeability sub-domains via the control volumes that span the sub-domain boundaries. This leakage results in a delayed saturation front when compared to the HyCVFE solution. N_{CVFE} and N_{HyCVFE} used to model this problem are 2912 and 3060, respectively. Fig. 8e shows the wetting phase migrates into the low permeability zone towards the right-hand end of the fracture in the HyCVFE method only after the displacing phase reaches the intermediate permeability outlet zone.

We compare the normalized mass leakage of the proposed HyCVFE method (Fig. 9a) and the discontinuous approach of Salinas et al. [35] (Fig. 9b) against the classical CVFE method; leakage using both methods is approximately two orders of magnitude lower than for the CVFE approach. The normalized mass leakage results from Salinas et al. [35] were obtained using a 3D model but can be compared with our 2D results because the material properties of the model cross-section were simply extruded into the third dimension so the model was effectively 2D. We extract the number of degrees of freedom (Dof) required for the classical CVFE method on a given 2D mesh (N_{CVFE}), and use this as a reference against which to compare the number of DoF required by the new HyCVFE method (N_{HyCVFE}) and the discontinuous method of Salinas et al. [35] ($N_{Salinas}$) for the same mesh. This allows us to cross-compare the DoF required for the different methods. Fig. 9c shows the resulting cross-plot of N_{HyCVFE} and $N_{Salinas}$ against N_{CVFE}. The unit slope on this plot corresponds to the case where the new hybrid or discontinuous method requires the same number of DoF as the classical CVFE method for a given mesh. The discontinuous method of Salinas et al. [35] plots on a line which lies considerably above the unit slope, because the method requires 18 degrees of freedom per 2D element. In contrast, the new HyCVFE method plots almost exactly on the unit slope, showing that the number of additional DoF required by the method is insignificant compared to the classical CVFE approach on a given mesh. Thus, although both methods are effective in reducing mass leakage, the proposed HyCVFE approach requires far fewer additional DoF because the discontinuity between elements is applied locally, rather than globally as in Salinas et al. [35].

4.4. Embedded box problem

We now consider the embedded box example from Abushaikha et al. [4]. The two-dimensional model is comprised of a low permeability box embedded in a high permeability region via a sharp interface with permeability contrast of 4 orders

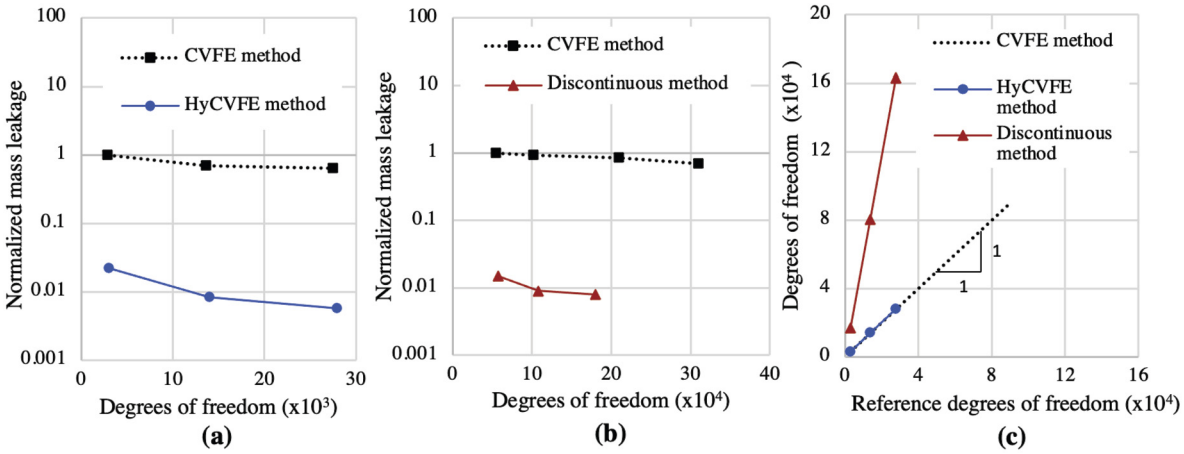

Fig. 9. (a-b) Comparison of the normalized mass leakage as a function of the number of DoF for the single fracture test case (4.3). **(a)** Two-dimensional model for HyCVFE and CVFE at 0.1 PVI. **(b)** Three-dimensional model using discontinuous and CVFE methods from Salinas et al. [35]. **(c)** cross-plot of N_{HyCVFE} and $N_{Salinas}$ against N_{CVFE} for the 2D fracture model. The unit slope is the reference for the computational requirements of the classical CVFE method.

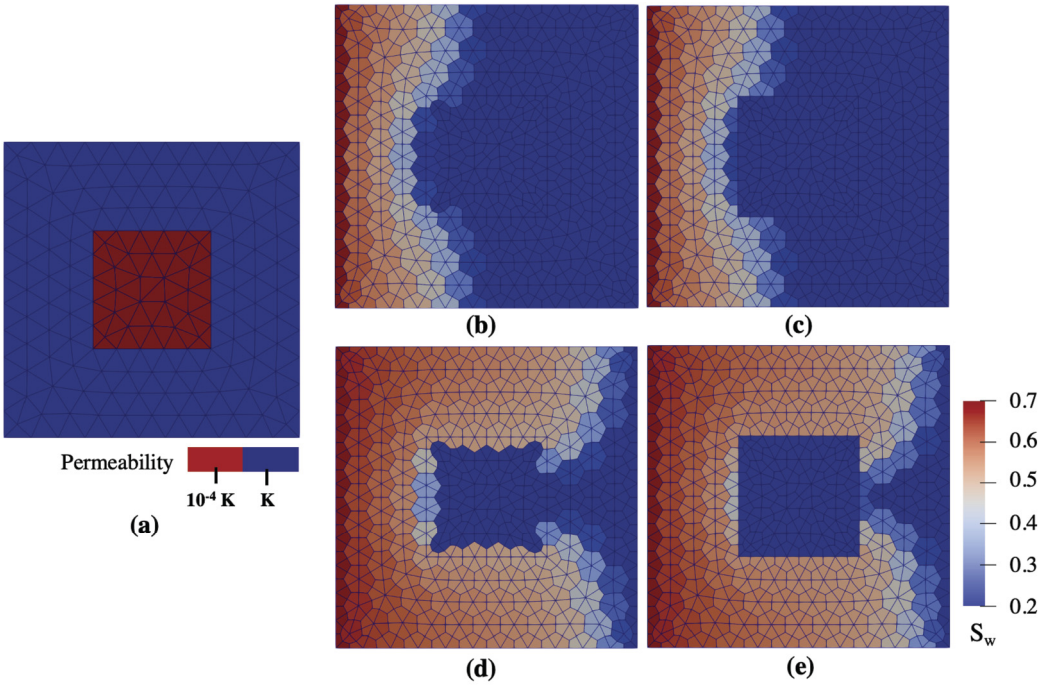

Fig. 10. (**a**) The permeability field of the embedded box test case (4.4). The contrast in the permeability is 4 orders of magnitude between the embedded box and the external region. (**b** – **e**) Comparison of the saturation solution displayed using the control volume representation. The middle column shows the CVFE method while the right column shows the HyCVFE method. (**b**) and (**c**) are the saturation solutions of the CVFE and the HyCVFE methods, respectively, after 0.12 PVI. (**d**) and (**e**) show the saturation solutions of the CVFE and the HyCVFE methods, respectively, after 0.25 PVI.

of magnitude (Table 1). The permeability field is shown in Fig. 10a. Constant pressure boundary conditions are applied on the left and right boundaries, and the wetting phase is injected over the left boundary. The top and bottom boundaries are no-flow. Comparisons of the saturation solutions between the HyCVFE and CVFE methods are shown in Fig. 10(b-e) at two timesteps, after 0.12 and 0.25 PVI. The saturation solution in the outer region is in good agreement between the two methods after 0.12 PVI. However, after 0.25 PVI the CVFE method displays non-physical leakage of the saturation solution across the discontinuous material interface, due to the continuous control volumes that span the interface. In this numerical example, N_{CVFE} and N_{HyCVFE} are 966 and 1006, respectively. Fig. 11a compares the normalized mass leakage for different mesh refinements. The HyCVFE approach shows several orders of magnitude less mass leakage in the saturation solution when compared with the reference CVFE method. Furthermore, we compare the computational requirements on the cross plot in Fig. 11b. Similar to the previous example, the slope of the N_{HyCVFE} method is very close to the unit slope,

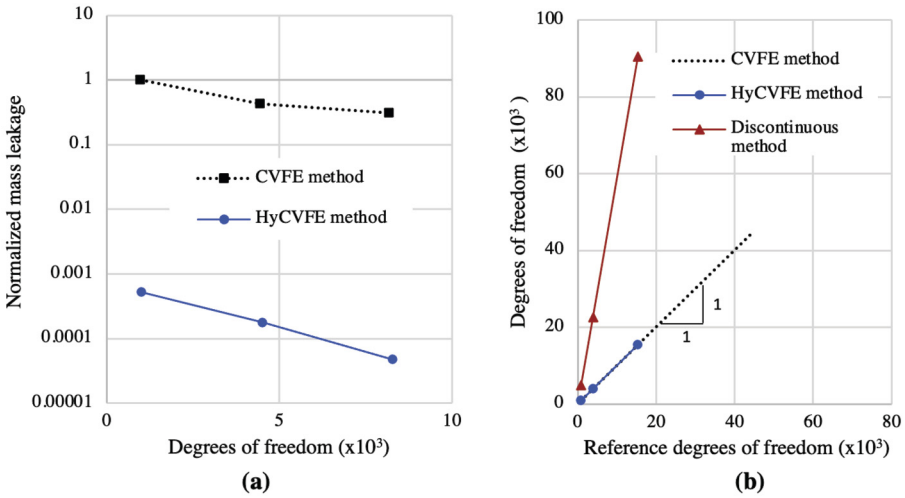

Fig. 11. The embedded box test case (4.4). (**a**) Comparison of the normalized mass leakage as a function of Dof for HyCVFE and CVFE methods at 0.2 PVI. (**b**) cross-plot of N_{HyCVFE} and $N_{Salinas}$ against N_{CVFE} for the embedded box model. The unit slope is the reference for the computational requirements of the classical CVFE method.

demonstrating that the additional DoF required for the HyCVFE approach are negligible when compared to the discontinuous method of Salinas et al. [35].

4.5. Wedge pinch out problem

This final case comprises of a high permeability wedge or fracture that pinches out. The tip of the wedge is made up of a few elements with large aspect ratio. The model represents the complex geometry of many geological systems and presents a challenge for accurate and efficient modeling [26]. The permeability contrast between the sub-domains is 6 orders of magnitude (Fig. 12a and Table 1). We apply constant pressure boundary conditions on the left and right boundaries with no flow through the top and bottom boundaries and inject the wetting phase over the left boundary. The saturation distribution is displayed at two time steps in Fig. 12(b-e). After 0.014 PVI, the wetting phase reaches the tip of the wedge in the HyCVFE approach while the CVFE method displays a slower flow of the wetting phase through the wedge due to mass leakage into the surrounding low permeability domain via the control volumes that span the boundary. The wetting phase in the CVFE approach takes more than twice as long to reach the wedge tip at 0.034 PVI.

The (N_{CVFE}) and (N_{HyCVFE}) used to model this case are 874 and 920, respectively. The normalized mass leakage is approximately one order of magnitude lower for the HyCVFE method (Fig. 13a), yet the computational cost is similar and much smaller again than the discontinuous method of Salinas et al. [35]. Fig. 13b shows the cross plot of the number of N_{HyCVFE} and $N_{Salinas}$ against N_{CVFE}. Unlike the HyCVFE approach that does not require many additional DoF, the Salinas et al. [35] method again has a steep slope indicating the high computational cost for a given mesh with respect to the reference CVFE method. This case emphasizes the appropriate application of the HyCVFE method where the sub-domains are meshed according to the underlying material geometry without influencing the adjacent region or the need to apply mesh refinement to capture accurate multiphase flow behaviours.

5. Conclusions

The proposed HyCVFE formulation is a promising numerical method for simulating multiphase flow problems in highly heterogeneous porous media that require geometrically complex models discretized using unstructured meshes. The approach has the following advantages: 1) The element pair $P_{0,DG} - P_{1,H}$ provides stable numerical solutions for coupled flow and transport problems. 2) The discretization of the continuity equation in the HyCVFE approach yields locally and globally mass conservative solutions. 3) The formulation exploits the efficient continuous pressure approximation in sub-domains with uniform or smoothly varying material properties. The continuous control volumes constructed by spanning element boundaries within sub-domains are desirable for efficiency. 4) Along material property discontinuities that correspond to sub-domain boundaries, additional nodes are applied to preserve sharp saturation changes over the interface based on a discontinuous pressure approximation. These nodes prevent control volumes from spanning multiple sub-domains and thus reduce mass leakage. 5) The general approach of the HyCVFE formulation is well suited to incorporate additional physics such as gravitational and capillary forces and rock and fluid compressibility. Including these physics is the topic of future work. 6) The approach can be readily extended from 2D to 3D models by populating hybrid nodes on the vertices of the tetrahedral faces separating the sub-domains. In common with most investigations of new numerical methods, the HyCVFE approach is currently implemented in a 'proof of concept' 2D code; in future work, we will investigate the performance

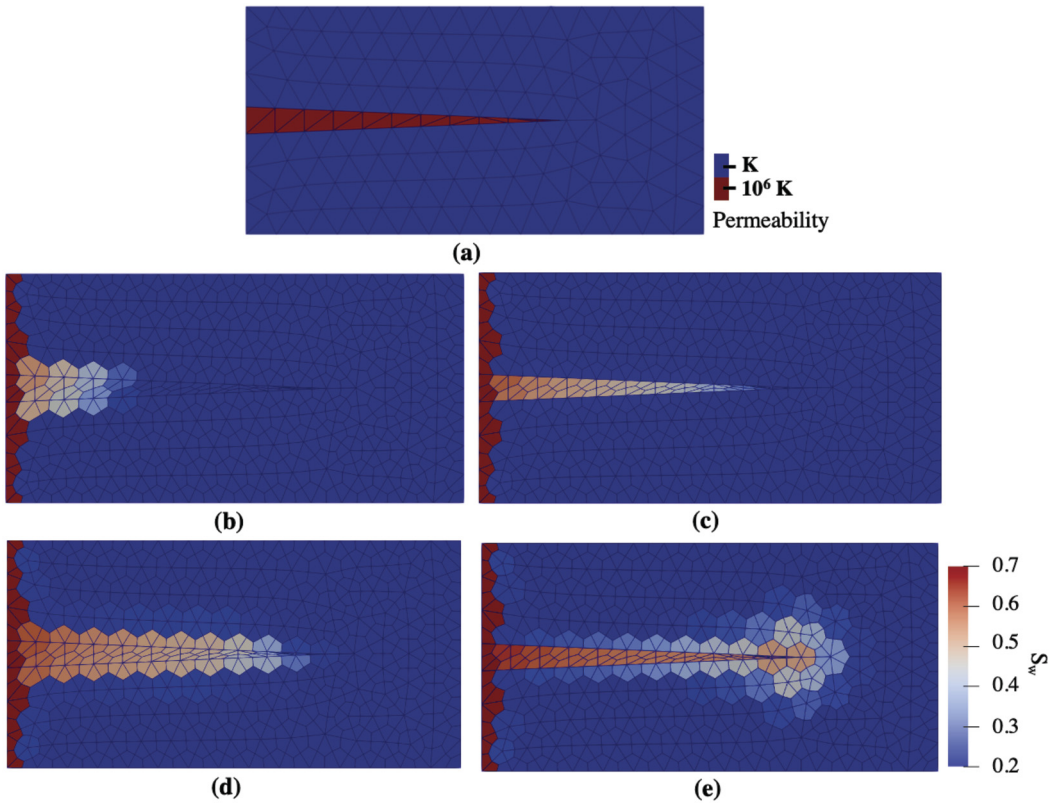

Fig. 12. **(a)** The permeability field of the wedge test case (4.5) with the contrast in permeability of 6 orders of magnitude. The tip of the wedge pinch out is made up of several elements with large aspect ratio. **(b-e)** Comparison of the saturation solution of the fracture problem displayed using the control volume representation. The left column shows the CVFE method while the right column shows HyCVFE method. **(b)** and **(c)**, **(d)** and **(e)** display the solution after 0.014 and 0.034 PVI, respectively.

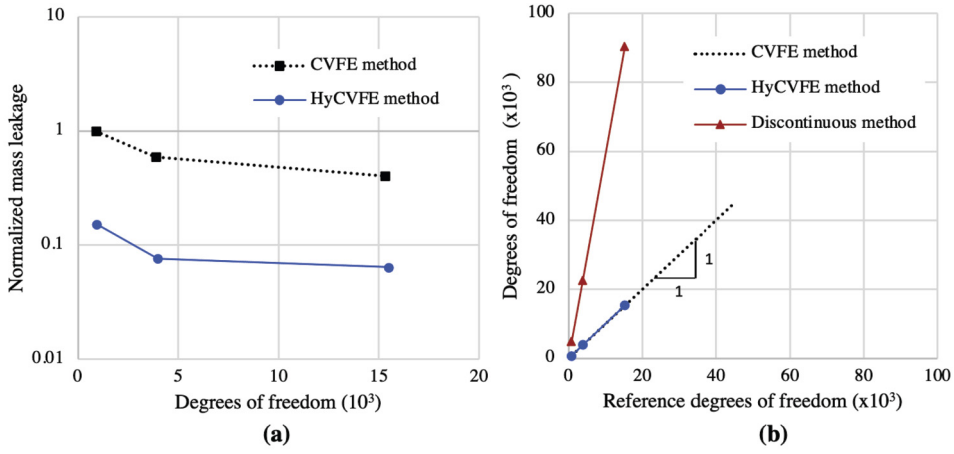

Fig. 13. **(a)** Comparison of the normalized mass leakage as a function of DoF for the HyCVFE and CVFE methods in the wedge test case (4.5) at 0.014 PVI. **(b)** cross-plot of N_{HyCVFE} and $N_{Salinas}$ against N_{CVFE} for the wedge model. The unit slope is the reference for the computational requirements of the classical CVFE method.

of the method in large 3D domains with parallel implementation. 7) The gains in accuracy far outweigh the overhead of additional computational cost to use this hybrid approach. The numerical examples show that only 4-5% of additional degrees of freedom are introduced and provide significant improvements, up to several orders of magnitude, to the solution accuracy.

CRediT authorship contribution statement

Jumanah Al Kubaisy: Conceptualization, Methodology, Software, Validation, Visualization, Writing – original draft. **Pablo Salinas:** Conceptualization, Methodology, Writing – review & editing. **Matthew D. Jackson:** Supervision, Writing – review & editing.

Declaration of competing interest

The authors declare that they have no known competing financial interests or personal relationships that could have appeared to influence the work reported in this paper.

Data availability

No data was used for the research described in the article.

Acknowledgements

Funding for Al Kubaisy from Saudi Aramco, and for Salinas and Jackson from the UK Engineering and Physical Sciences Research Council (EPSRC, grant reference EP/R01938X/1) is gratefully acknowledged.

References

[1] I. Aavatsmark, An introduction to multipoint flux approximations for quadrilateral grids, Comput. Geosci. 6 (2002) 405–432, https://doi.org/10.1023/A:1021291114475.
[2] I. Aavatsmark, T. Barkve, Ø. Bøe, T. Mannseth, Discretization on non-orthogonal, curvilinear grids for multi-phase flow, EarthDoc URL: https://www.earthdoc.org/content/papers/10.3997/2214-4609.201411179, https://doi.org/10.3997/2214-4609.201411179, 1994.
[3] I. Aavatsmark, T. Barkve, Ø. Bøe, T. Mannseth, Discretization on non-orthogonal, quadrilateral grids for inhomogeneous, anisotropic media, J. Comput. Phys. 127 (1996) 2–14, https://doi.org/10.1006/jcph.1996.0154.
[4] A.S. Abushaikha, M.J. Blunt, O.R. Gosselin, C.C. Pain, M.D. Jackson, Interface control volume finite element method for modelling multi-phase fluid flow in highly heterogeneous and fractured reservoirs, J. Comput. Phys. 298 (2015) 41–61, https://doi.org/10.1016/j.jcp.2015.05.024, https://www.sciencedirect.com/science/article/pii/S0021999115003587.
[5] A.S. Abushaikha, K.M. Terekhov, A fully implicit mimetic finite difference scheme for general purpose subsurface reservoir simulation with full tensor permeability, J. Comput. Phys. 406 (2020) 109194, https://doi.org/10.1016/j.jcp.2019.109194, https://www.sciencedirect.com/science/article/pii/S002199911930899X.
[6] I. Avaatsmark, T. Barkve, Ø. Bøe, T. Mannseth, A class of discretization methods for structured and unstructured grids in anisotropic, inhomogeneous media, European Association of Geoscientists and Engineers URL: https://www.earthdoc.org/content/papers/10.3997/2214-4609.201406875, https://doi.org/10.3997/2214-4609.201406875, 1996.
[7] K. Aziz, A. Settari, Petroleum Reservoir Simulation, Applied Science Publishers, 1979.
[8] P. Bastian, R. Helmig, Efficient fully-coupled solution techniques for two-phase flow in porous media: parallel multigrid solution and large scale computations, Adv. Water Resour. 23 (1999) 199–216, https://doi.org/10.1016/S0309-1708(99)00014-7, https://www.sciencedirect.com/science/article/pii/S0309170899000147.
[9] R.H. Brooks, A.T. Corey, Hydraulic properties of porous media and their relation to drainage design, Trans. ASABE 7 (1964) 26–0028.
[10] S. Buckley, M. Leverett, Mechanism of fluid displacement in sands, Trans. AIME 146 (1942) 107–116, https://doi.org/10.2118/942107-G, https://onepetro.org/TRANS/article-pdf/146/01/107/2177908/spe-942107-g.pdf.
[11] G. Chavent, G. Cohen, J. Jaffre, M. Dupuy, I. Ribera, Simulation of two-dimensional waterflooding by using mixed finite elements, Soc. Pet. Eng. J. 24 (1984) 382–390, https://doi.org/10.2118/10502-PA, https://onepetro.org/spejournal/article-pdf/24/04/382/2653226/spe-10502-pa.pdf.
[12] G. Chavent, G. Cohen, J. Jaffré, R. Eymard, D.R. Guérillot, L. Weill, Discontinuous and mixed finite elements for two-phase incompressible flow, SPE Reserv. Eng. 5 (1990) 567–575, https://doi.org/10.2118/16018-PA, https://onepetro.org/RE/article-pdf/5/04/567/2629131/spe-16018-pa.pdf.
[13] G. Chavent, J. Roberts, A unified physical presentation of mixed, mixed-hybrid finite elements and standard finite difference approximations for the determination of velocities in waterflow problems, Adv. Water Resour. 14 (1991) 329–348, https://doi.org/10.1016/0309-1708(91)90020-O, https://www.sciencedirect.com/science/article/pii/030917089190020O.
[14] P. Deveugle, M.D. Jackson, G. Hampson, M. Farrell, A. Sprague, J. Stewart, C. Calvert, Characterization of stratigraphic architecture and its impact on fluid flow in a fluvial-dominated deltaic reservoir analog: Upper Cretaceous Ferron Sandstone Member, Utah, AAPG Bull. 95 (2011) 693–727, https://doi.org/10.1306/09271010025.
[15] J. Douglas Jr., Finite difference methods for two-phase incompressible flow in porous media, SIAM J. Numer. Anal. 20 (1983) 681–696, https://doi.org/10.1137/0720046.
[16] L.J. Durlofsky, A triangle based mixed finite element–finite volume technique for modeling two phase flow through porous media, J. Comput. Phys. 105 (1993) 252–266, https://doi.org/10.1006/jcph.1993.1072.
[17] L.J. Durlofsky, Accuracy of mixed and control volume finite element approximations to Darcy velocity and related quantities, Water Resour. Res. 30 (1994) 965–973, https://doi.org/10.1029/94WR00061, https://agupubs.onlinelibrary.wiley.com/doi/abs/10.1029/94WR00061, https://agupubs.onlinelibrary.wiley.com/doi/pdf/10.1029/94WR00061.
[18] M.G. Edwards, Unstructured, control-volume distributed, full-tensor finite-volume schemes with flow based grids, Comput. Geosci. 6 (2002) 433–452, https://doi.org/10.1023/A:1021243231313.
[19] M.G. Edwards, Higher-resolution hyperbolic-coupled-elliptic flux-continuous CVD schemes on structured and unstructured grids in 3-D, Int. J. Numer. Methods Fluids 51 (2006) 1079–1095, https://doi.org/10.1002/fld.1289, https://onlinelibrary.wiley.com/doi/abs/10.1002/fld.1289, https://onlinelibrary.wiley.com/doi/pdf/10.1002/fld.1289.
[20] P.A. Forsyth, A control volume finite element approach to NAPL groundwater contamination, SIAM J. Sci. Stat. Comput. 12 (1991) 1029–1057, https://doi.org/10.1137/0912055.
[21] L.S.K. Fung, A.D. Hiebert, L.X. Nghiem, Reservoir simulation with a control-volume finite-element method, SPE Reserv. Eng. 7 (1992) 349–357, https://doi.org/10.2118/21224-PA, https://onepetro.org/RE/article-pdf/7/03/349/2611950/spe-21224-pa.pdf.

[22] S. Geiger, S. Roberts, S.K. Matthäi, C. Zoppou, A. Burri, Combining finite element and finite volume methods for efficient multiphase flow simulations in highly heterogeneous and structurally complex geologic media, Geofluids 4 (2004) 284–299, https://doi.org/10.1111/j.1468-8123.2004.00093.x, https://onlinelibrary.wiley.com/doi/abs/10.1111/j.1468-8123.2004.00093.x, https://onlinelibrary.wiley.com/doi/pdf/10.1111/j.1468-8123.2004.00093.x.
[23] J.L.M.A. Gomes, D. Pavlidis, P. Salinas, Z. Xie, J.R. Percival, Y. Melnikova, C.C. Pain, M.D. Jackson, A force-balanced control volume finite element method for multi-phase porous media flow modelling, Int. J. Numer. Methods Fluids 83 (2017) 431–445, https://doi.org/10.1002/fld.4275, https://onlinelibrary.wiley.com/doi/abs/10.1002/fld.4275, https://onlinelibrary.wiley.com/doi/pdf/10.1002/fld.4275.
[24] G.H. Graham, M.D. Jackson, G.J. Hampson, Three-dimensional modeling of clinoforms in shallow-marine reservoirs: part 1. Concepts and application, AAPG Bull. 99 (2015) 1013–1047, https://doi.org/10.1306/01191513190, https://pubs.geoscienceworld.org/aapgbull/article-pdf/99/6/1013/3378809/BLTN13190.pdf.
[25] R. Helmig, R. Huber, Comparison of Galerkin-type discretization techniques for two-phase flow in heterogeneous porous media, Adv. Water Resour. 21 (1998) 697–711, https://doi.org/10.1016/S0309-1708(97)00023-7, https://www.sciencedirect.com/science/article/pii/S0309170897000237.
[26] M.D. Jackson, J.R. Percival, P. Mostaghimi, B.S. Tollit, D. Pavlidis, C.C. Pain, J.L. Gomes, A.H. El-Sheikh, P. Salinas, A.H. Muggeridge, M.J. Blunt, Reservoir modeling for flow simulation by use of surfaces, adaptive unstructured meshes, and an overlapping-control-volume finite-element method, SPE Reserv. Eval. Eng. 18 (2015) 115–132, https://doi.org/10.2118/163633-PA, https://onepetro.org/REE/article-pdf/18/02/115/2127830/spe-163633-pa.pdf.
[27] C. Jacquemyn, M.D. Jackson, G.J. Hampson, Surface-based geological reservoir modelling using grid-free NURBS curves and surfaces, Math. Geosci. 51 (2019) 1–28, https://doi.org/10.1007/s11004-018-9764-8.
[28] S.K. Matthäi, A. Mezentsev, M. Belayneh, Finite element–node-centered finite-volume two-phase-flow experiments with fractured rock represented by unstructured hybrid-element meshes, SPE Reserv. Eval. Eng. 10 (2007) 740–756, https://doi.org/10.2118/93341-PA, https://onepetro.org/REE/article-pdf/10/06/740/2559431/spe-93341-pa.pdf.
[29] R. Mosé, P. Siegel, P. Ackerer, G. Chavent, Application of the mixed hybrid finite element approximation in a groundwater flow model: luxury or necessity?, Water Resour. Res. 30 (1994) 3001–3012, https://doi.org/10.1029/94WR01786, https://agupubs.onlinelibrary.wiley.com/doi/abs/10.1029/94WR01786, https://agupubs.onlinelibrary.wiley.com/doi/pdf/10.1029/94WR01786.
[30] S. Nardean, M. Ferronato, A.S. Abushaikha, A novel block non-symmetric preconditioner for mixed-hybrid finite-element-based Darcy flow simulations, J. Comput. Phys. 442 (2021) 110513, https://doi.org/10.1016/j.jcp.2021.110513, https://www.sciencedirect.com/science/article/pii/S0021999121004083.
[31] H. Nick, S. Matthäi, A hybrid finite-element finite-volume method with embedded discontinuities for solute transport in heterogeneous media, Vadose Zone J. 10 (2011) 299–312, https://doi.org/10.2136/vzj2010.0015, https://acsess.onlinelibrary.wiley.com/doi/abs/10.2136/vzj2010.0015, https://acsess.onlinelibrary.wiley.com/doi/pdf/10.2136/vzj2010.0015.
[32] H.M. Nilsen, K.A.A. Lie, J.R. Natvig, Accurate modeling of faults by multipoint, mimetic, and mixed methods, SPE J. 17 (2012) 568–579, https://doi.org/10.2118/149690-PA, https://onepetro.org/SJ/article-pdf/17/02/568/2097674/spe-149690-pa.pdf.
[33] H. Osman, G.H. Graham, A. Moncorge, C. Jacquemyn, M.D. Jackson, Is cell-to-cell scale variability necessary in reservoir models?, Math. Geosci. 53 (2021) 571–596, https://doi.org/10.1007/s11004-020-09877-y.
[34] D.W. Peaceman, Fundamentals of Numerical Reservoir Simulation, Elsevier Scientific Pub. Co.: Distributors for the U.S. and Canada, Elsevier North-Holland, Amsterdam; New York, 1977, pp. 2–5, chapter 1.
[35] P. Salinas, D. Pavlidis, Z. Xie, H. Osman, C. Pain, M. Jackson, A discontinuous control volume finite element method for multi-phase flow in heterogeneous porous media, J. Comput. Phys. 352 (2018) 602–614, https://doi.org/10.1016/j.jcp.2017.09.058, https://www.sciencedirect.com/science/article/pii/S0021999117307313.
[36] K. Schmid, S. Geiger, K. Sorbie, Higher order FE–FV method on unstructured grids for transport and two-phase flow with variable viscosity in heterogeneous porous media, J. Comput. Phys. 241 (2013) 416–444, https://doi.org/10.1016/j.jcp.2012.12.017, https://www.sciencedirect.com/science/article/pii/S0021999112007486.
[37] J.R. Shewchuk, Delaunay refinement algorithms for triangular mesh generation, in: 16th ACM Symposium on Computational Geometry, Comput. Geom. 22 (2002) 21–74, https://doi.org/10.1016/S0925-7721(01)00047-5, https://www.sciencedirect.com/science/article/pii/S0925772101000475.
[38] L. Tran, J. Kim, S. Matthäi, Simulation of two-phase flow in porous media with sharp material discontinuities, Adv. Water Resour. 142 (2020) 103636, https://doi.org/10.1016/j.advwatres.2020.103636, https://www.sciencedirect.com/science/article/pii/S030917081931214X.
[39] C. van Duijn, M. de Neef, Similarity solution for capillary redistribution of two phases in a porous medium with a single discontinuity, Adv. Water Resour. 21 (1998) 451–461, https://doi.org/10.1016/S0309-1708(97)00012-2, https://www.sciencedirect.com/science/article/pii/S0309170897000122.
[40] N. Zhang, A.S. Abushaikha, An efficient mimetic finite difference method for multiphase flow in fractured reservoirs, in: SPE Europec Featured at EAGE Conference and Exhibition, Day 2 Tue, June 04, 2019, 2019, https://onepetro.org/SPEEURO/proceedings-pdf/19EURO/2-19EURO/D021S001R011/1174632/spe-195512-ms.pdf.
[41] N. Zhang, A.S. Abushaikha, Fully implicit reservoir simulation using mimetic finite difference method in fractured carbonate reservoirs, in: SPE Reservoir Characterisation and Simulation Conference and Exhibition, Day 2 Wed, September 18, 2019, 2019, https://onepetro.org/SPERCSC/proceedings-pdf/19RCSC/2-19RCSC/D021S010R003/1178790/spe-196711-ms.pdf.